Effect of implementing magnetic resonance imaging for patient-specific OpenSim models on lower-body kinematics and knee ligament lengths

Effect of implementing magnetic resonance imaging for patient-specific OpenSim models on lower-body kinematics and knee ligament lengths

Kenneth B. Smale[1], Michele Conconi[2], Nicola Sancisi[2], Michael Krogsgaard[3], Tine Alkjaer[4], Vincenzo Parenti Castelli[2], Daniel L. Benoit[1,5]

[1] Faculty of Health Sciences, University of Ottawa, Canada

[2] Faculty of Industrial Engineering, University of Bologna, Italy

[3] Section for Sports Traumatology M51, Bispebjerg-Frederiksberg Hospital, Denmark

[4] Department of Physical and Occupational Therapy, Copenhagen University Hospital

[5] Department of Biomedical Sciences, University of Copenhagen, Denmark

Corresponding Author:

Daniel Benoit
200 Lees Avenue
Ottawa, Canada
K1S 5S9
Tel: 1-613-562-5800 x 8547
dbenoit@uottawa.ca

Key Words: biomechanics, computer simulation, knee injuries, musculoskeletal model

Abstract

Background: OpenSim models are typically based on cadaver findings that are generalized to represent a wide range of populations, which curbs their validity. Patient-specific modelling through incorporating magnetic resonance imaging (MRI) improves the model's biofidelity with respect to joint alignment and articulations, muscle wrapping, and ligament insertions. The purpose of this study was to determine if the inclusion of an MRI-based knee model would elicit differences in lower limb kinematics and resulting knee ligament lengths during a side cut task.

Methods: Eleven participants were analyzed with the popular Rajagopal OpenSim model, two variations of the same model to include three and six degrees of freedom knee (DOF), and a fourth version featuring a four DOF MRI-based knee model. These four models were used in an inverse kinematics analysis of a side cut task and the resulting lower limb kinematics and knee ligament lengths were analyzed.

Results: The MRI-based model was more responsive to the movement task than the original Rajagopal model while less susceptible to soft tissue artifact than the unconstrained six DOF model. Ligament isometry was greatest in the original Rajagopal model and smallest in the six DOF model.

Conclusions: When using musculoskeletal modelling software, one must acutely consider the model choice as the resulting kinematics and ligament lengths are dependent on this decision. The MRI-based knee model is responsive to the kinematics and ligament lengths of highly dynamic tasks and may prove to be the most valid option for continuing with late-stage modelling operations such as static optimization.

Introduction

Simulation software such as OpenSim (Delp et al., 2007) provides a modeling environment where individual variables (muscle and ligament parameters, kinematics, etc.) can be manipulated and the outcomes of these interventions examined to identify cause-and-effect relationships. In silico models have been effective in identifying the ligament and contact roles during knee motion (Nardini et al., 2016; Sancisi and Parenti-Castelli, 2011). OpenSim in silico models have also been used to determine muscle force contributions (Delp et al., 1990; Hamner et al., 2010) and knee joint contact loads (Fregly et al., 2011) during walking and running.

Although these human movement simulations have advanced our knowledge of the neuromuscular and skeletal systems, they still exhibit limitations that affect their validity. For example, in silico models are primarily based on in vitro cadaver studies (Delp et al., 1990; Hamner et al., 2010; Rajagopal et al., 2016) leading to a somewhat generic application of muscle parameters, bone geometry, and joint articulations. OpenSim models (Arnold et al., 2010; Rajagopal et al., 2016) have attempted to address the biofidelity of the knee joint by enhancing the OpenSim one degree of freedom (DOF) hinge joint to one that prescribes motion based on cadaveric work (Walker et al., 1988). In these models, knee flexion/extension is unprescribed, while the remaining five DOF are a function of this sagittal plane angle. Although this is more anatomically accurate than a simple hinge joint, it still lacks consideration of patient-specific bone geometries and their respective articulation.

Since muscle force and joint contact load estimations are higher level analyses in the OpenSim program flow, errors and inaccuracies in earlier analyses are propagated and perhaps multiplied when using these late-stage tools. OpenSim analyses begin with scaling to match the

model's anthropometric and inertial properties to each individual participant. Once completed, the model undergoes inverse kinematics, which steps through the trial frame by frame and positions the scaled OpenSim model so that it best matches the experimental markers. This best match is defined by a minimization of a sum of weighted squares algorithm in which the weights of each marker are user-defined. Therefore, trying to fit a generic model to patient-specific experimental data during scaling or inverse kinematics is likely to induce error in the results. Comparisons of generic and patient-specific models have demonstrated this with knee joint contact forces being more accurately modeled using patient-specific parameters (Gerus et al., 2013; Lerner et al., 2015). One type of patient-specific model incorporates magnetic resonance imaging (MRI) data to customize and improve bone geometry, muscle wrapping, and ligament lengths (Conconi et al., 2018). Although MRIs can be included in OpenSim (Schmid et al., 2009; Valente et al., 2017), it remains unclear how an MRI-based knee model would affect lower limb kinematics and ligament lengths during dynamic tasks.

To address this knowledge gap, the purpose of this study was to determine if the inclusion of an MRI-based knee model would elicit differences in lower limb kinematics and resulting knee ligament lengths during a side cut task. Among the many kinematic models previously proposed in the literature (Leardini et al., 2017), three have been chosen to compare a patient-specific MRI-based model: the standard Rajagopal model and two other Rajagopal models adapted to contain three and six unprescribed knee DOF. The three DOF version was included as this is how the knee is commonly represented in other models such as the Plug-In Gait and is a progressive benchmark between the one and six DOF models. The six DOF model was included as a true in vivo knee is known to have six unconstrained (3 rotations and 3 translations) DOF. It was hypothesized that the original Rajagopal model would result in the

smallest range of motion while the unconstrained six DOF model would have the largest range of motion for both kinematics and ligament lengths. It was further anticipated that the MRI-based model would reduce the range of motion observed in six DOF model but range of motion would still be larger during the side cut task than the original Rajagopal model.

Methods

In vivo data

This in silico work was based on 11 anterior cruciate ligament (ACL) deficient patients (4 female, 7 male; 28.3 ± 5.4 years; 175.1 ± 8.5 cm; 77.2 ± 14.3 kg). Inclusion criteria included primary ACL injury and no history of contralateral ACL ruptures. This study was approved by the Capital Region of Denmark and University of Ottawa ethics committees.

Participants were outfitted with a whole-body cluster marker set (Mantovani and Lamontagne, 2016) with kinematic data being collected at 100 Hz by a 10-camera motion capture system (6 MX and 4 T series, Vicon, UK). To successfully complete the side cut task, participants performed the movement as fast as they could, cutting onto and off of the force plate with their injured leg at 45 ± 10° angles marked by taping on the floor. Three to four successful side cuts were recorded for each participant. The side cut was chosen over simpler tasks such as gait because this movement is multiplanar and induces forces that would stress the validity of the unconstrained six DOF and prescribed Walker knee functions that were developed in a low-load, in vitro flexion-extension movement. Furthermore, since movements such as gait are not typically associated with injury, we chose to examine a task that is known to be associated with ACL injury (Boden et al., 2000).

All data were processed with MatLab (2015b, Mathworks, USA) and OpenSim (3.3, Simtk, USA). Marker trajectories were filtered with a 4th order zero-lag low pass Butterworth filter with a cut-off frequency of 15 Hz. The side cut movement was time normalized to 100% stance phase with the addition of 10% stance time prior to initial contact. Thus, the movement spans from -10% stance to 100% stance.

OpenSim Models

Four OpenSim models were compared in this study, differing only by model employed for the knee joint: (1) the original Rajagopal (RO) model (Rajagopal et al., 2016); (2) the RO with all three rotational knee DOFs unprescribed and three translational DOF locked to zero (R3); (3) six DOF system (R6) using the six DOF motion boundaries presented by Xu et al. (2013); (4) a six DOF MRI-based model (RM; discussed below). The overall musculoskeletal models were subjected to the same scaling procedure using identical measurement sets and scale factors, independently from the employed knee joint. Joint coordinate systems and motions of all models were expressed according to International Society of Biomechanics standards (Wu and Cavanagh, 1995).

MRI Acquisition and Analysis

MRI images were taken with 1.5 Tesla, repetition time/echo time: 500/14 ms, field of view: 18 cm, and slice thickness: 3 mm (Sigma Horizon LX 1.5 Tesla, General Electric, USA). Combinations of frontal and sagittal views of T1 and T2-weighted scans including fat-saturated versions were used to segment the femur, tibia, and fibula (Workbench 2016.11, MITK, Germany). Femoral and tibial insertion sites for the anterior and posterior cruciate ligaments and

medial and lateral collateral ligaments were designated as point clouds on their respective surfaces.

The three-dimensional segmented bones were then loaded into Rhinoceros (4.0, McNeel & Associates, USA) along with a generic femur and tibia. These full-length generic bones were aligned with the deprecated MRI bones so that coordinates for the hip and ankle joint centers could be obtained. This alignment was performed with the function *Orient3Pt*, which uses the knee joint center, medial epicondyle and hip joint center markers to align the MRI and generic bones in three-dimensional space. Once the MRI and generic bones were aligned, the same anatomical points as above from the scaled whole-body OpenSim model were loaded into Rhinoceros and used to align the MRI/generic markers to their corresponding OpenSim model matches. To summarize, this process allows us to take the deprecated MRI bones, estimate hip and ankle joint centers, and align the knee joint and anatomical points to the OpenSim reference system. Therefore, all anatomical landmarks used in the inverse kinematics process were based on the experimental markers but the generic femur, tibia, and fibula were exchanged for the aligned MRI versions.

Construction of MRI patient-specific (RM) Model

To define the patient-specific parameters of the RM model the natural motion[1] of each participant was first computed similar to Conconi et al. (2018, 2015) as the envelope of tibiofemoral configurations that minimize the peak contact pressure, i.e. that maximize joint congruence (Conconi and Parenti-Castelli, 2014). This approach has been validated with in-vitro testing (Forlani et al., 2016) and sensibility analyses proving its stability (Conconi et al., 2015).

[1] The natural motion is the motion that the articulation exhibits when no work is done to deform the joint passive structures. Experimentally, it can be measured by moving the articulation with the smallest loads possible. It is thus overlap with the definition of passive motion proposed in (Wilson et al., 2000).

The articular surfaces obtained from MRIs were approximated with four spheres: two for the femoral and two for the tibial condyles. The radius and position of the centers of these initial spheres were then optimized (max variation allowed: ± 2 mm) in order to guarantee both the medial and lateral contact over the entire natural knee motion (Figure 1). Previous studies have shown how this simplified approach can successfully replicate the kinematic constraint imposed by condylar contacts (Nardini et al., 2016; Sancisi and Parenti-Castelli, 2011). The optimized spheres were introduced into the RM model and, assuming that both the condyles remain in contact during the considered task, converted into two constant length constraints between the femoral and tibial sphere centers in both the medial and lateral knee compartments. Due to the concave and convex nature of the medial and lateral tibia plateaus, respectively, the contact sphere centers are proximal for the medial sphere and distal for the lateral sphere with respect to the tibia origin (Figure 2).

The origin and insertion of the ACL, PCL, MCL, and LCL of each participant were also determined as those associated with the most isometric fiber of the respective ligament (Victor et al., 2009; Wilson et al., 1998). These origins and insertions of the four knee ligaments were incorporated into all four models but were used solely to analyze the ligament elongation and not used as kinematic constraints. Even though all patients had a complete ACL rupture, these lengths were still included as an exploratory analysis due to the ligament's insertions still being discernible in the MRIs.

Inverse and Point Kinematics

Inverse kinematics was performed on each trial with the four individual models. The same marker weightings were maintained between the models so that tracking errors satisfied the

guidelines as outlined by Hicks et al. (2015). Point kinematics is an OpenSim tool that determines model marker trajectories in the reference system of choice (i.e. global or local). This analysis was executed to procure the ligaments' tibial insertion coordinates with respect to the femoral coordinate system. These coordinates were then used to determine the ligament lengths over the entire side cutting trial.

Statistical Analysis

To test for significance between the four models, repeated measures ANOVAs were applied through statistical parametric mapping (Pataky, 2010) for each hip, knee, and ankle DOF. If the F statistic was found to be significant, a post-hoc analysis of paired sample t-tests with a Bonferroni correction were used to determine between which models the significant differences occurred. All tests were deemed significant if $p < 0.05$. To determine the clinical relevance of these differences, Cohen's *d* effect sizes were calculated during the peak difference between the two models. A $d = 0.2$ is considered small, 0.5 considered medium, and $d = 0.8$ considered large (Cohen, 2013). All statistical analyses were performed in MatLab.

Results

For the sake of brevity, only significant differences between RM and the other three models with medium or larger ($d > 0.5$) effect sizes are reported.

Kinematics

The only DOF to have clinically relevant effect sizes between RM and the other three models were knee adduction/abduction, knee internal/external rotation, and the three knee translations (Figure 3).

RM resulted in knee abduction angles for the majority of stance while the other three models resulted in knee adduction. RM differed from RO between 6 - 93% stance ($p < 0.0001$) with the peak difference of 4.52° ($d = 2.01$). RM also differed from R3 between -10 - 93% stance ($p < 0.0001$) with the peak difference of 5.16° ($d = 1.51$). Finally, RM differed from R6 between -10 - 84% stance ($p < 0.0001$) with the peak difference of 6.59° ($d = 2.12$). Finally, clinically relevant significant differences in knee internal/external rotation were noted between RM and RO. RO was significantly more internally rotated between -10 – 55% of stance ($p < 0.0001$) with a peak difference of 11.42° ($d = 2.58$).

With respect to translations, the RM tibia was significantly more posterior than the RO tibia between -10 – 62% of stance ($p < 0.0001$) with a peak difference of 3.7 mm ($d = 1.12$). Differences between R6 and RM were even greater as RM was more posterior between -10 – 88% ($p < 0.0001$) and 98 – 100% ($p = 0.021$) stance with the peak difference of 10.8 mm ($d = 3.00$). Knee medial/lateral translation was similar between R6 and RM but RM was significantly more lateral than RO between -10 – 100% stance ($p < 0.0001$) with the peak difference of 2.4 mm ($d = 2.15$). Finally, RM was significantly different from both RO and R6 models in knee distraction/compression. RM followed the same pattern as RO but was significantly more distracted between 61 – 85% of stance ($p = 0.014$) with a peak difference of 3.6 mm ($d = 0.67$). RM was significantly difference from -10 – 8% ($p = 0.018$), 48 – 71% ($p < 0.0001$), and 84 – 100% ($p = 0.023$) stance with a peak difference of 5.4 mm ($d = 0.92$).

The introduction of a MRI-based model with a constant length constraint appears to not only reduce the oscillations in translational DOFs but also eliminate bone overlapping (Figure 4). This overlapping is especially apparent in R6 as the constant lengths derived from the MRI spheres show up to 15 mm of deviation from these lengths.

Ligament Lengths

There were no clinically relevant significant differences between RM and the RO and R3 models for any ligaments (effect size ranges from d = 0.70 to 1.29). However, the ACL length significantly differed between RM and R6 from -10 – 3% ($p < 0.0001$), 30 – 72% ($p = 0.008$), and 91 – 100% ($p < 0.0001$) stance. The peak difference between these three periods was 9.8 mm ($d = 1.29$). For the PCL length, RM significantly differed from R6 between 13 - 75% ($p < 0.0001$) and 99 – 100% ($p = 0.028$) stance with a peak difference of 5.0 mm ($d = 0.70$). For the MCL length, RM significantly differed from R6 between 16 – 79% ($p < 0.0001$) and 95 – 100% ($p < 0.0001$) stance with a peak difference of 7.9 mm ($d = 0.99$). Finally, LCL length differed between RM and R6 between 31 – 72% ($p = 0.006$) and 97 – 100% ($p = 0.011$) stance with a peak difference of 7.3 mm ($d = 0.75$).

Discussion

The goal of the current study was to determine if a patient-specific model elicits differences in lower limb kinematics and resulting ligament lengths during a side cut movement compared to generic OpenSim models. The patient-specific MRI model showed significantly different kinematics (Figure 3) especially in knee adduction/abduction and translations. Ligament lengthening during the side cut was also found to be significantly different (Figure 5) between the patient-specific and generic models.

Kinematics

As expected with respect to knee translations, the R6 model produced non-physiologically high translations (Figure 3) and appeared to be influenced by soft tissue artefact, which is manifested as oscillations following initial contact (Smale et al., 2017). These

oscillations were effectively mitigated by the current MRI based model due to the constant contact length constraints and resulted in a smoothing of translations similar to that observed by our previous work using bone-pin derived kinematics applied to OpenSim models (Smale et al., 2017). Although generic OpenSim models visually describe articulating bone geometry as solid shapes, inverse kinematics does not treat them as such and therefore may solve for joint positions with considerable overlap of bones (Figure 6). The femoral and tibial knee joint center origin compression (overlapping) was reduced by the MRI-based knee model compared to the unprescribed six DOF model (Figure 4) and therefore appears to provide more physiological inverse kinematics solutions.

Kinematic error whether caused by soft tissue artifact or anatomically inaccurate models has a major impact on the clinical relevance of the findings. Hewett and colleagues (2005) observed knee abduction angles at landing to be 8.4° greater in females that later went on to suffer an ACL injury, whereas Krosshaug and colleagues (2007) observed knee abduction angles of 7 ± 1.5° at the time of ACL rupture during video analyses. Considering the generic models (RO, R3, and R6) all resulted in knee adduction during this side cut while the patient-specific model (RM) resulted in a peak difference of 4.5° that placed the knee in abduction, these studies may be underestimating the true amount of knee abduction associated with ACL injury due to kinematic error. These differences therefore highlight the importance of choosing an appropriate kinematic model and knowing the limitations of the applied model, particularly when the results will be used for clinical applications.

As previously mentioned, the Walker kinematic functions are based on cadaveric specimens but also only experience a 7.5 kg simulated quadriceps force to the specimens when producing flexion and extension motions (Harding et al., 1977). Therefore, the Walker

prescribed functions were not developed with considering movements in the frontal and transverse plane, which are known to occur during many dynamic tasks such as walking or side cuts. Furthermore, given the large ground reaction forces during side cuts, expected whole-body rotations in the global lab space, and that loading alters knee joint kinematics (Andriacchi and Dyrby, 2005; Benoit et al., 2007), it appears as though the functions derived through the cadaveric work of Walker et al (1988) may be unsuitable for highly dynamic tasks such as the side cutting movement.

Ligament Lengths

In vivo dynamic MRI studies indicate that ACL and PCL lengths range from 25 to 35 mm in length throughout knee flexion during a quasi-static lunge (Li et al., 2017), while the MCL and LCL ranged from 65 – 90 mm and 45 – 60 mm in length, respectively (Park et al., 2006). Our estimated lengths for RM fall within the high end of those ranges for all four ligaments. During dynamic tasks, human knee ligaments typically have in vivo strain values ranging up to 5% original ligament length (Luque-Seron and Medina-Porqueres, 2016). The ligaments in the current model are kinematically driven, meaning their ligament force is determined by the amount of strain they exhibit. Thus, our results indicate that the lack of change in RO ligament lengths may underestimate ligament strain and ultimately true ligament force, while the R6 may result in overestimating ligament strain and true force. The R3 or RM models would therefore seem the most biofidelic approach when using static optimization to derive ligament forces. Ligaments are not generally included in OpenSim inverse kinematics models as they are considered as passive and kinematically-driven elements. A simple one DOF model would produce ligament lengths based solely on flexion angle while the current MRI patient-specific models allow for unconstrained tibiofemoral motion while avoiding unrealistic joint

displacements. Thus, this more advanced model provides more biofidelic ligament length estimates, which in turn leads to more realistic strain values in later analyses.

Limitations

Even though ligament insertions sites on the MRI are identified as point clouds, a single point within these clouds to produce the most isometric fiber of each ligament is used to determine the optimum insertion points and length. This naturally leads to a more conservative estimate in length changes but was a necessary assumption when trying to implement patient-specific parameters into an OpenSim model. A more advanced MRI analysis that considers multiple bundles for each ligament would likely yield a more detailed model but is beyond the scope of this study.

A second limitation is associated with the relatively small framing of the MRIs. These images were originally intended for diagnostic purposes and therefore do not include the full femur, tibia, and fibula. Although we aligned femur and tibia bone sections to another full MRI bone set, we could not account for individual femoral neck anteversion and tibial torsion, which could affect hip and ankle joint positions. It should be stressed however that the MRI knee joints were aligned to the experimental markers obtained through motion capture so that even though the exact joint center positions are unknown, patient-specific anatomical landmarks were used for their alignment.

A third limitation is that even though considerable differences were observed amongst the four different models, the actual in vivo motions remain unknown. Based on current in vivo research (Potvin et al., 2017; Smale et al., 2017) and the reduction of soft tissue artifact using the RM model, we believe that it is the most biofidelic; however, when deciding which model to use

in OpenSim we recommend evaluating the costs and benefits of biofidelity and analysis time, which are always based on the research question to be answered.

A fourth limitation is the use of spherical approximations for the two condylar contacts. Spherical and planar simplification has been widely employed in the past when modelling the knee (Abdel-Rahman and Hefzy, 1998; Sancisi and Parenti-Castelli, 2011; Wilson and O'Connor, 1997). In particular, Parenti-Castelli and Di Gregorio (2000) have shown how it is possible to define a parallel mechanism, whose links replicate the constraints exerted by ligaments and spherical approximation of the contacts. Moreover, increasing the complexity of contacts representation from simple spheres to higher order surfaces did not improve the model's capability to replicate the knee motion (Ottoboni et al., 2010). Thus, the sphere-on-sphere contact may be considered as a valid representation of the kinematic constraints exerted by the condylar contact. In particular, this simplification becomes less severe if the sphere's geometry and thus the kinematic constraint is optimized about a reference motion, as done in the current paper.

Conclusion

Our MRI-based knee model and Opensim analysis (1) allows users to evaluate three unprescribed knee joint rotations and translations during a highly ballistic side cut task, (2) attenuates soft tissue artifact, and (3) results in physiological tibiofemoral motions and ligament length estimates. We also found that results obtained from generic knee joint models contain errors that limit their interpretation and application with respect to secondary knee joint motions and ligament deformation in patient populations. Those limitations, combined with our results and existing in vivo knee joint kinematic data, call into question the validity of existing knee

injury mechanics literature. Our work also underscores the importance of choosing the most biofidelic model possible within the limitations of a researcher's resources since the resulting kinematics and ligament lengths are dependent on this decision. It is clear from our study that model choice will have a significant impact on the study outcome measures and thus clinical significance of the results.

Acknowledgments

The authors would like to thank Dr. Teresa Flaxman, Ida Fillingsnes, and Louise Jorgensen for their help during data collections. Thank you also to Drs. Mohammad Sharif Shourijeh and Fabrizio Nardini for their help in establishing OpenSim setup files and coordinate transformation matrices. The authors would also like to thank the Natural Sciences and Engineering Research Council (NSERC) of Canada and the Erasmus Mundus Nova Domus programs for their financial support of KB Smale. Finally, the authors would like to thank the Lundbeck Foundation, Ase and Ejnar Danielsens Fund, and the Danish Rheumatism Foundation for their financial support in the form of operating grants.

Conflict of Interest

The authors have no conflicts of interest to declare.

References

Abdel-Rahman, E.M., Hefzy, M.S., 1998. Three-dimensional dynamic behaviour of the human knee joint under impact loading. Med. Eng. Phys. 20, 276–290.

Andriacchi, T.P., Dyrby, C.O., 2005. Interactions between kinematics and loading during walking for the normal and ACL deficient knee. J. Biomech. 38, 293–298. https://doi.org/10.1016/j.jbiomech.2004.02.010

Arnold, E.M., Ward, S.R., Lieber, R.L., Delp, S.L., 2010. A Model of the Lower Limb for Analysis of Human Movement. Ann. Biomed. Eng. 38, 269–279.

Benoit, D.L., Ramsey, D.K., Lamontagne, M., Xu, L., Wretenberg, P., Renström, P., 2007. In vivo knee kinematics during gait reveals new rotation profiles and smaller translations. Clin. Orthop. 454, 81–88. https://doi.org/10.1097/BLO.0b013e31802dc4d0

Boden, B.P., Dean, G.S., Feagin Jr, J.A., Garrett Jr, W.E., 2000. Mechanisms of anterior cruciate ligament injury. Orthopedics 23, 573–578.

Cohen, J., 2013. Statistical Power Analysis for the Behavioral Sciences. Routledge.

Conconi, M., Castelli, V.P., 2014. A sound and efficient measure of joint congruence. Proc. Inst. Mech. Eng. [H] 228, 935–941. https://doi.org/10.1177/0954411914550848

Conconi, M., Leardini, A., Parenti-Castelli, V., 2015. Joint kinematics from functional adaptation: A validation on the tibio-talar articulation. J. Biomech. 48, 2960–2967. https://doi.org/10.1016/j.jbiomech.2015.07.042

Conconi, M., Sancisi, N., Parenti-Castelli, V., 2018. Subject-Specific Model of Knee Natural Motion: A Non-invasive Approach, in: Advances in Robot Kinematics 2016, Springer Proceedings in Advanced Robotics. Springer, Cham, pp. 255–264. https://doi.org/10.1007/978-3-319-56802-7_27

Delp, S.L., Anderson, F.C., Arnold, A.S., Loan, P., Habib, A., John, C.T., Guendelman, E., Thelen, D.G., 2007. OpenSim: open-source software to create and analyze dynamic simulations of movement. IEEE Trans. Biomed. Eng. 54, 1940–1950. https://doi.org/10.1109/TBME.2007.901024

Delp, S.L., Loan, P., Hoy, M.G., Zajac, F.E., Topp, E.L., Rosen, J.M., 1990. An Interactive Graphics-Based Model of the Lower Extremity to Study Orthopaedic Surgical Procedures. IEEE Trans. Biomed. Eng. 37.

Forlani, M., Sancisi, N., Conconi, M., Parenti-Castelli, V., 2016. A new test rig for static and dynamic evaluation of knee motion based on a cable-driven parallel manipulator loading system. Meccanica 51, 1571–1581. https://doi.org/10.1007/s11012-015-0124-1

Fregly, B.J., Besier, T.F., Lloyd, D.G., Delp, S.L., Banks, S.A., Pandy, M.G., D'Lima, D.D., 2011. Grand Challenge Competition to predict in vivo knee loads. J. Orthop. Res.

Gerus, P., Sartori, M., Besier, T.F., Fregly, B.J., Delp, S.L., Banks, S.A., Pandy, M.G., D'Lima, D.D., Lloyd, D.G., 2013. Subject-specific knee joint geometry improves predictions of medial tibiofemoral contact forces. J. Biomech. 46, 2778–2786. https://doi.org/10.1016/j.jbiomech.2013.09.005

Hamner, S.R., Seth, A., Delp, S.L., 2010. Muscle contributions to propulsion and support during running. J. Biomech. 43, 2709–2716. https://doi.org/10.1016/j.jbiomech.2010.06.025

Harding, M.L., Harding, L., Goodfellow, J.W., 1977. A preliminary report of a simple rig to aid study of the functional anatomy of the cadaver human knee joint. J. Biomech. 10, 517–523.

Hewett, T.E., Myer, G.D., Ford, K.R., Heidt, R.S., Colosimo, A.J., McLean, S.G., van den Bogert, A.J., Paterno, M.V., Succop, P., 2005. Biomechanical measures of neuromuscular control and valgus loading of the knee predict anterior cruciate ligament injury risk in female athletes: a prospective study. Am. J. Sports Med. 33, 492–501. https://doi.org/10.1177/0363546504269591

Hicks, J.L., Uchida, T.K., Seth, A., Rajagopal, A., Delp, S.L., 2015. Is my model good enough? Best practices for verification and validation of musculoskeletal models and simulations of movement. J. Biomech. Eng. 137.

Krosshaug, T., Nakamae, A., Boden, B.P., Engebretsen, L., Smith, G., Slauterbeck, J.R., Hewett, T.E., Bahr, R., 2007. Mechanisms of anterior cruciate ligament injury in basketball: video analysis of 39 cases. Am. J. Sports Med. 35, 359–367. https://doi.org/10.1177/0363546506293899

Leardini, A., Belvedere, C., Nardini, F., Sancisi, N., Conconi, M., Parenti-Castelli, V., 2017. Kinematic models of lower limb joints for musculo-skeletal modelling and optimization in gait analysis. J. Biomech. 62, 77–86. https://doi.org/10.1016/j.jbiomech.2017.04.029

Lerner, Z.F., DeMers, M.S., Delp, S.L., Browning, R.C., 2015. How tibiofemoral alignment and contact locations affect predictions of medial and lateral tibiofemoral contact forces. J. Biomech. 48, 644–650. https://doi.org/10.1016/j.jbiomech.2014.12.049

Li, G., DeFrate, L.E., Sun, H., Gill, T.J., 2017. In Vivo Elongation of the Anterior Cruciate Ligament and Posterior Cruciate Ligament during Knee Flexion. Am. J. Sports Med. https://doi.org/10.1177/0363546503262175

Luque-Seron, J.A., Medina-Porqueres, I., 2016. Anterior Cruciate Ligament Strain In Vivo: A Systematic Review. Sports Health 8, 451–455. https://doi.org/10.1177/1941738116658006

Mantovani, G., Lamontagne, M., 2016. How Different Marker Sets Affect Joint Angles in Inverse Kinematics Framework. J. Biomech. Eng. https://doi.org/10.1115/1.4034708

Nardini, F., Sancisi, N., Belvedere, C., Conconi, M., Leardini, A., Castelli, V.P., 2016. Definition of a subject-specific model of the knee in vivo. Gait Posture 49, S6. https://doi.org/10.1016/j.gaitpost.2016.07.030

Ottoboni, A., Parenti-Castelli, V., Sancisi, N., Belvedere, C., Leardini, A., 2010. Articular surface approximation in equivalent spatial parallel mechanism models of the human knee joint: an experiment-based assessment. Proc. Inst. Mech. Eng. [H] 224, 1121–1132. https://doi.org/10.1243/09544119JEIM684

Parenti-Castelli, V., Di Gregorio, R., 2000. Parallel Mechanisms Applied to the Human Knee Passive Motion Simulation, in: Lenarčič, J., Stanišić, M.M. (Eds.), Advances in Robot Kinematics. Springer Netherlands, Dordrecht, pp. 333–344. https://doi.org/10.1007/978-94-011-4120-8_35

Park, S.E., DeFrate, L.E., Suggs, J.F., Gill, T.J., Rubash, H.E., Li, G., 2006. Erratum to "The change in length of the medial and lateral collateral ligaments during in vivo knee flexion." The Knee 13, 77–82. https://doi.org/10.1016/j.knee.2004.12.012

Pataky, T.C., 2010. Generalized n-dimensional biomechanical field analysis using statistical parametric mapping. J. Biomech. 43, 1976–1982. https://doi.org/10.1016/j.jbiomech.2010.03.008

Potvin, B.M., Shourijeh, M.S., Smale, K.B., Benoit, D.L., 2017. A practical solution to reduce soft tissue artifact error at the knee using adaptive kinematic constraints. J. Biomech. 62, 124–131. https://doi.org/10.1016/j.jbiomech.2017.02.006

Rajagopal, A., Dembia, C.L., DeMers, M.S., Delp, D.D., Hicks, J.L., Delp, S.L., 2016. Full-Body Musculoskeletal Model for Muscle-Driven Simulation of Human Gait. IEEE Trans. Biomed. Eng. 63, 2068–2079. https://doi.org/10.1109/TBME.2016.2586891

Sancisi, N., Parenti-Castelli, V., 2011. A novel 3D parallel mechanism for the passive motion simulation of the patella-femur-tibia complex. Meccanica 46, 207–220. https://doi.org/10.1007/s11012-010-9405-x

Schmid, J., Sandholm, A., Chung, F., Thalmann, D., Delingette, H., Magnenat-Thalmann, N., 2009. Musculoskeletal Simulation Model Generation from MRI Data Sets and Motion Capture Data, in: Recent Advances in the 3D Physiological Human. Springer, London, pp. 3–19. https://doi.org/10.1007/978-1-84882-565-9_1

Smale, K.B., Potvin, B.M., Shourijeh, M.S., Benoit, D.L., 2017. Knee joint kinematics and kinetics during the hop and cut after soft tissue artifact suppression: Time to reconsider ACL injury mechanisms? J. Biomech. 62, 132–139. https://doi.org/10.1016/j.jbiomech.2017.06.049

Valente, G., Crimi, G., Vanella, N., Schileo, E., Taddei, F., 2017. nmsBuilder: Freeware to create subject-specific musculoskeletal models for OpenSim. Comput. Methods Programs Biomed. 152, 85–92. https://doi.org/10.1016/j.cmpb.2017.09.012

Victor, J., Wong, P., Witvrouw, E., Sloten, J.V., Bellemans, J., 2009. How isometric are the medial patellofemoral, superficial medial collateral, and lateral collateral ligaments of the knee? Am. J. Sports Med. 37, 2028–2036. https://doi.org/10.1177/0363546509337407

Walker, P.S., Rovick, J.S., Robertson, D.D., 1988. The effects of knee brace hinge design and placement on joint mechanics. J. Biomech. 21, 965–974. https://doi.org/10.1016/0021-9290(88)90135-2

Wilson, D.R., Feikes, J.D., O'Connor, J.J., 1998. Ligaments and articular contact guide passive knee flexion. J. Biomech. 31, 1127–1136.

Wilson, D.R., Feikes, J.D., Zavatsky, A.B., O'Connor, J.J., 2000. The components of passive knee movement are coupled to flexion angle. J. Biomech. 33, 465–473.

Wilson, D.R., O'Connor, J.J., 1997. A three-dimensional geometric model of the knee for the study of joint forces in gait. Gait Posture 5, 108–115. https://doi.org/10.1016/S0966-6362(96)01080-6

Wu, G., Cavanagh, P.R., 1995. ISB recommendations for standardization in the reporting of kinematic data. J. Biomech. 28, 1257–1261.

Xu, H., 2013. Development of a Musculoskeletal Model to Determine Knee Contact Force During Walking on Ballast Using Opensim Simulation. University of Utah, Utah, United States.

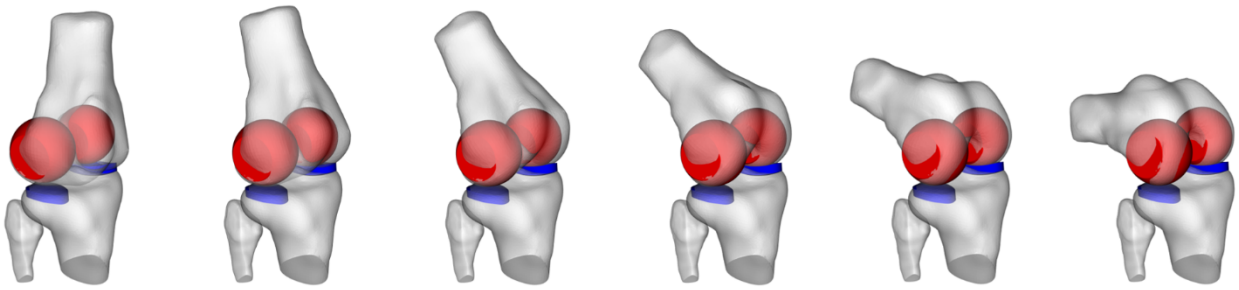

Figure 1.

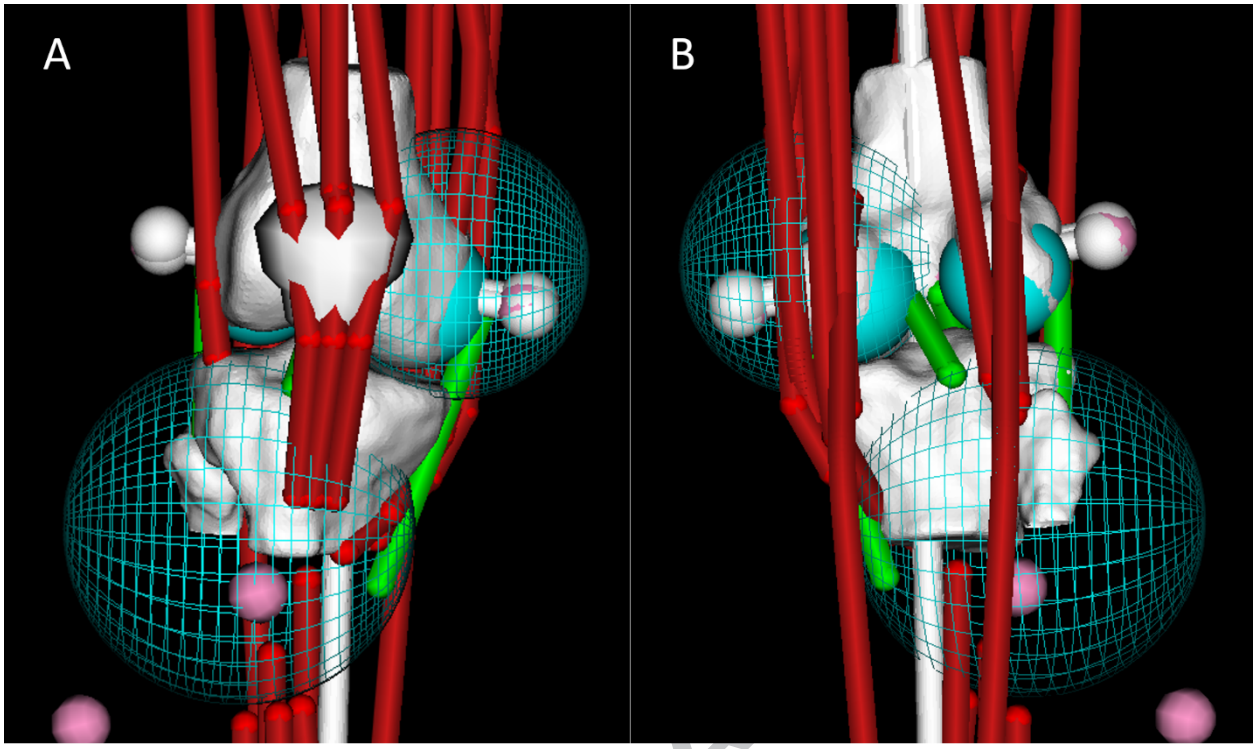

Figure 2.

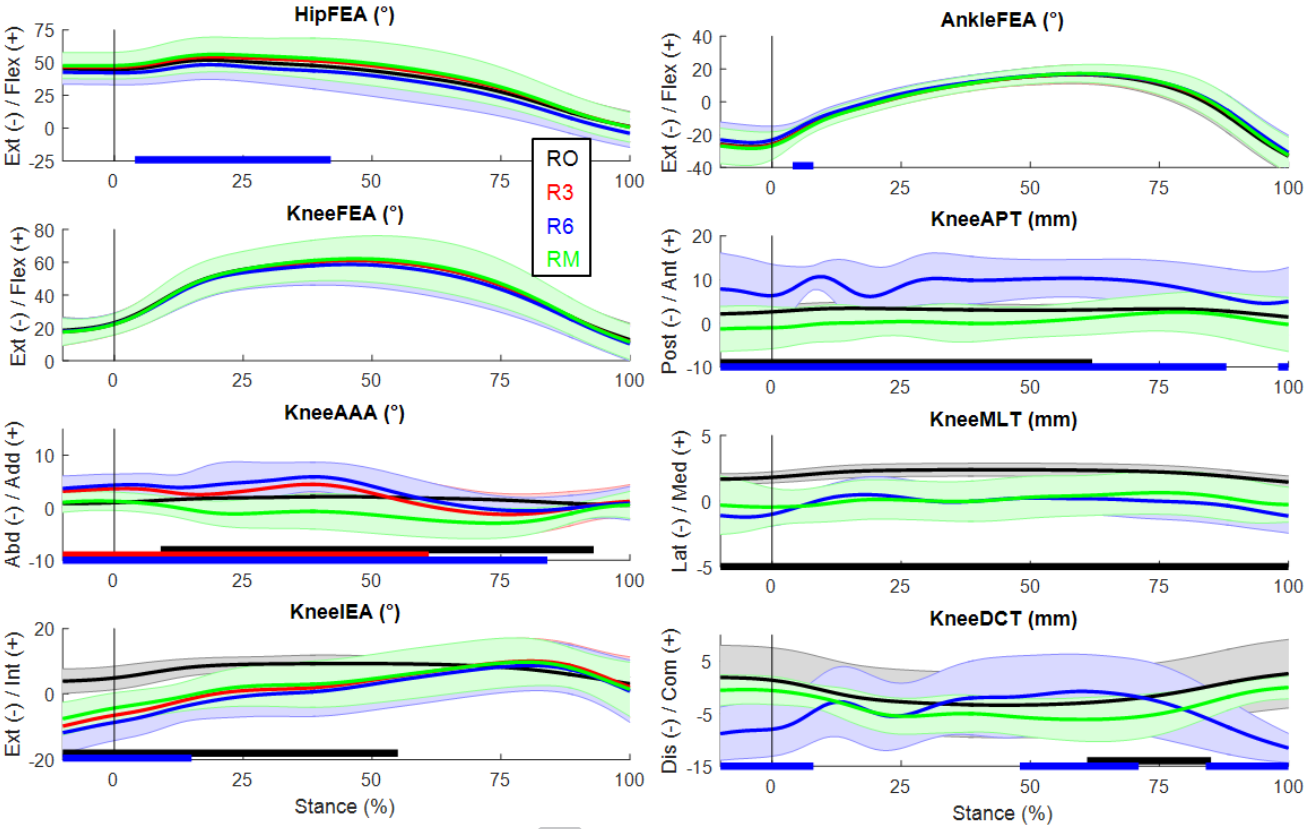

Figure 3.

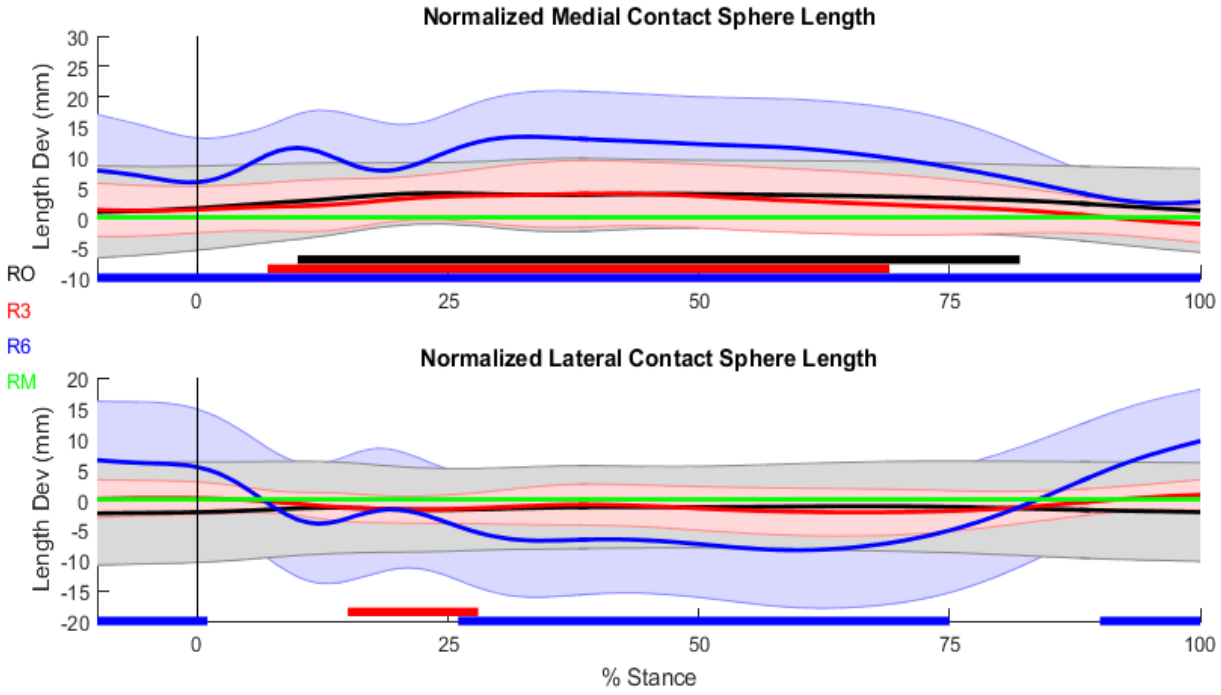

Figure 4.

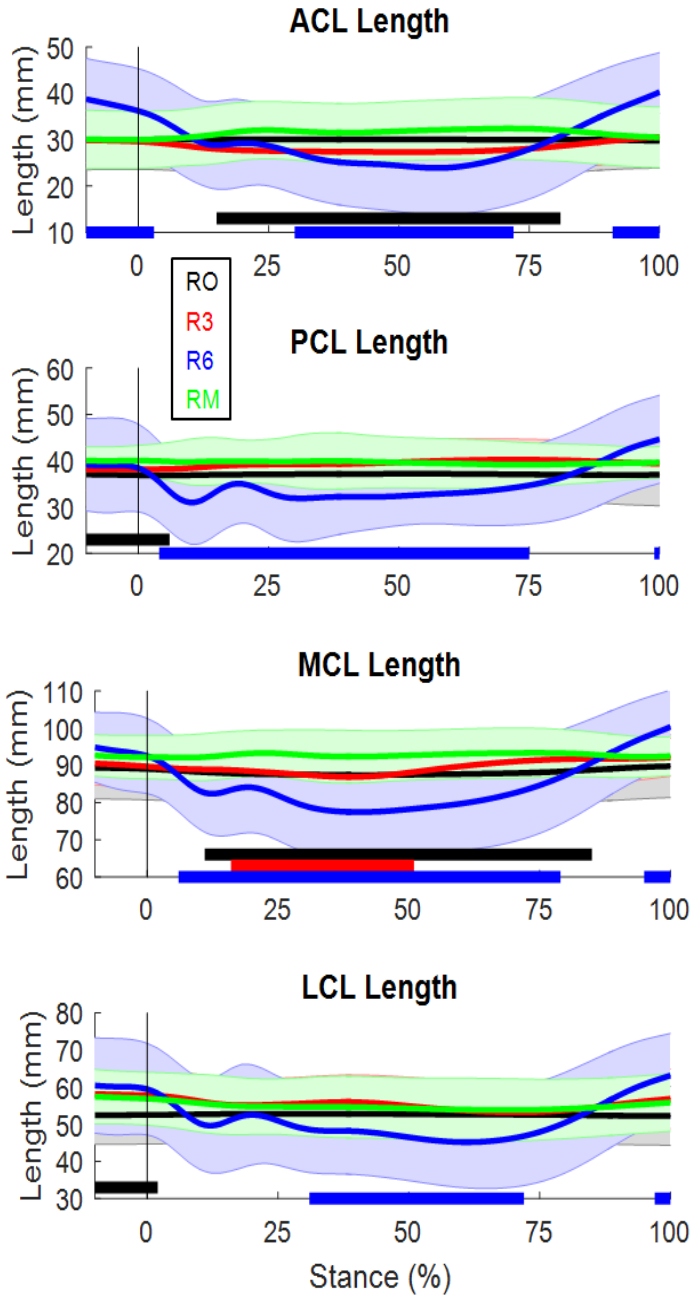

Figure 5.

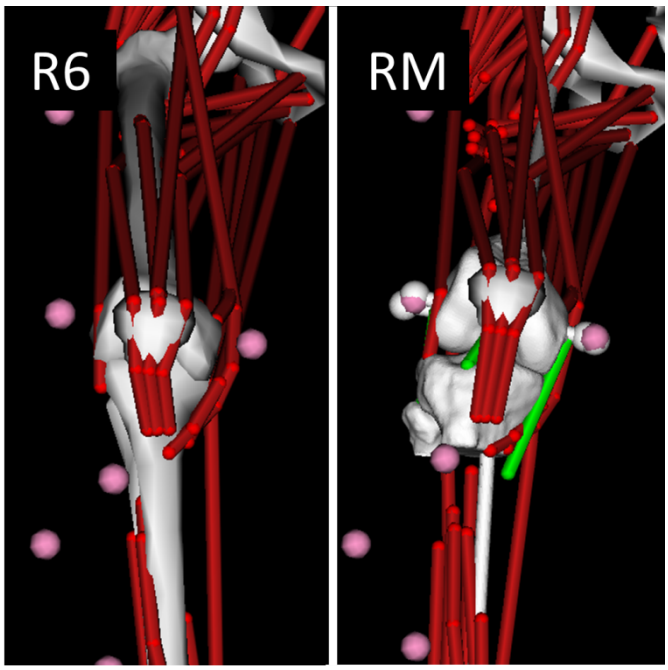

Figure 6.

Figure Captions

Figure 1. Example of natural congruence motion that ensures a constant medial and lateral contact lengths between the tibia and femur.

Figure 2. Anterior and posterior views of the MRI knee in which the femoral condyle spheres (solid teal) and tibial contact spheres (wired teal) are visible.

Figure 3. Kinematic means and standard deviation clouds of the side cut resulting from the four OpenSim models. Vertical bar represents initial contact while horizontal bars denote significance between RM and a respective model: RM vs RO (black), RM vs R3 (red), and RM vs R6 (blue). FEA, AAA, and IEA indicate flexion-extension, adduction-abduction, and internal-external rotation angles, respectively. APT, MLT, and DCT represent anterior-poster, medial-lateral, and distraction-compression translations, respectively.

Figure 4. Ligament lengths means and standard deviation clouds resulting from the four models. Vertical bar represents initial contact while horizontal bars denote significance between RM and other models: RM vs RO (black), RM vs R3 (red), and RM vs R6 (blue).

Figure 5. Demonstration of bone overlap in R6 model, which is eliminated in RM model.

Figure 6. Deviations of the four models from the contact sphere length derived from the MRI congruence motion. Values are presented as means and standard deviations through the side cut stance phase and represent co-penetration if negative and distraction if positive. Vertical bar represents initial contact while horizontal bars denote significance between RM and other models: RM vs RO (black), RM vs R3 (red), and RM vs R6 (blue).